Turk J Chem
36 (2012) , 55 – 67.

doi:10.3906/kim-1106-43

Ni_{55} nanocluster: a density functional theory study of the binding energy of nickel and ethylene adsorption

Nusret Duygu YILMAZER[1], Mehmet Ferdi FELLAH[2], Işık ÖNAL[1,*]
[1] *Department of Chemical Engineering, Middle East Technical University, 06800 Ankara-TURKEY*
e-mail: ional@metu.edu.tr
[2] *Department of Chemical Engineering, Yüzüncü Yıl University, 65080 Van-TURKEY*

Received: 17.06.2011

Ethylene adsorption on a Ni_{55} nanocluster was studied by means of the density functional theory (DFT)/B3LYP using the basis sets of 6-31G(d,p) and 86-411(41d)G in Gaussian 03. The Ni_{55} nanocluster was found to have a distorted icosahedral geometry, in accordance with the experimental findings. The binding energy value for the Ni_{55} nanocluster was calculated to be 3.51 eV/atom using equilibrium geometry calculations. The estimated bulk nickel binding energy was in reasonable agreement with the experimental value (4.85 versus 4.45 eV/atom). In addition, equilibrium geometry calculations were performed for ethylene adsorption on the Ni_{55} nanocluster for 2 different coordination numbers of 6 and 8 with π-adsorption modes. The related adsorption energies were computed as –0.87 and –0.68 eV, respectively.

Key Words: Ni_{55}, DFT, ethylene adsorption, nickel, coordination number, binding energy, nanocluster

Introduction

Developments in nanoscale science enable scientists to atomically engineer and characterize clusters of any size and composition. The importance of these developments lies in the fact that clusters offer a novel class of materials with electronic, catalytic, and magnetic properties that are different from the bulk.

According to a study by Grigoryan and Springborg,[1] nickel clusters that have N number of atoms in the range of 10-10,000 have interesting properties. In this particular work, different sizes of clusters were taken into consideration for a particular reaction in order to evaluate the effects that could be observed, since it was

*Corresponding author

claimed that the structure and properties of a cluster depend on N. Schmid et al.[2] emphasized that the basic reason for producing nanoparticle-based catalysts is to improve the ratio of the active surface to the total metal volume, where the catalytic properties change qualitatively with changes of the metal particle size.

An icosahedral structure was first identified for nickel clusters by looking at the size dependence of the chemical reactivity with various probe molecules.[3–5] Parks et al. experimentally investigated the structure of nickel clusters by use of ammonia[6] and nitrogen[7,8] adsorption on neutral nickel gas clusters for different cluster sizes ranging from 3 to 120 atoms. They reported that all of the nickel nanoclusters including Ni_{55} had Mackay icosahedral structures, and the magic-number clusters such as Ni_{13} and Ni_{55} were observed experimentally. Similarly, the icosahedral structure of Ni_{55} was found in a large mass range with threshold photoionization experiments and standard mass spectrometry by Pellarin et al.[5]

Chemical probe experiments on Ni clusters[6–9] showed icosahedral symmetry for $N > 48$. Parks and Riley[9] stated that bare nickel clusters in the size range of $49 \leq N \leq 105$ preferentially adopt icosahedral-based structures, and the experiments showed evidence of regular icosahedra and icosahedra with closed subshells.

There are many theoretical calculations on nickel clusters by a variety of techniques, including the methods based on density functional formalism. These are the embedded atom method (EAM),[10] the effective medium theory (EMT),[11] the corrected effective medium (CEM),[12] and tight-binding molecular dynamics (TBMD) and the linear combination of Gaussian-type orbitals-local density functional (LCGTO-LDF) method.[13] Lathiotakis et al.[13] studied Ni clusters with $N = 13$ and $N = 55$ by using the tight-binding (TB; semiempirical) molecular dynamics (MD) method. They reported that the most stable structure among these clusters was icosahedral. Moreover, Stave and DePristo[14] and Wetzel and DePristo[15] systematically computed energies and structures for nickel clusters containing 3-23 and 24-55 atoms by employing the CEM and MD/Monte Carlo-CEM (MD/MC-CEM) theories, respectively. Grigoryan and Springborg[1] studied the optimization of nickel clusters in the size range of N = 2-100 using the combination EAM (as developed by Daw, Baskes, and Foiles) and quasi-Newton optimization method. Grigoryan and Springborg[16] also utilized the EAM method in their calculations for Ni_N clusters in the size range of 2-150, where electronic effects like Jahn-Teller distortions were not included and a Mackay icosahedron was concluded as the structure for the Ni_{55} cluster. Montejano-Carrizales et al.[17] investigated icosahedral closed-shell clusters with N = 13, 55, 147, 309, ... , 5083. They concluded that the icosahedral structures were more stable at atom numbers up to N = 1415.

In another study by Montejano-Carrizales et al.,[18] Ni clusters in the size range of 13-147 were studied with EAM while keeping the cluster structure relaxed only up to N = 78; Jahn-Teller distortions were not included. In that work, 2 different types of structures based on icosahedral growth were considered, and a Mackay icosahedron was reported for the Ni_{55} cluster. Doye and Wales[19] used the Monte Carlo minimization approach for different metal clusters of up to 80 atoms without using Jahn-Teller distortions. They also reported that Ni_{55} nanoclusters had a Mackay icosahedral structure. Cleveland and Landman[20] worked on the energetics of nickel clusters. For Ni clusters containing fewer than 2300 atoms, the optimal structures of the clusters were predicted as icosahedral sequences. Ni nanoclusters were also studied by the MD method with a quantum-Sutten-Chen many-body force field.[21] For clusters with fewer than approximately 400 atoms, the most stable structure was reported to be an icosahedron.

In a study by Wang et al.,[22] distances of icosahedral Ni_{13} and Ni_{55} nanoclusters were discussed. Luo[23] adopted the TB approximation and the MD technique to compute the energies and structural properties of

nickel clusters containing 4-55 atoms and obtained an icosahedral structure for Ni_{13} and Ni_{55} as well. Kar'kin et al.[24] stated that Ni clusters with magic numbers N = 55 and N = 147 were energetically preferable within the chosen ranges of N. In this case, the structure of the ground state achieved during cooling corresponded to the Mackay icosahedron.

The Stariolo-Tsallis form of generalized simulated annealing (GSA) was applied to nickel clusters in order to determine the structures of Ni_N clusters (N = 2-55) in which the interatomic potentials were modeled by the Sutton-Chen version of fusion sensitivity (FS) potential.[25] In addition, structures of N = 13, 38, and 55 with high symmetry were concluded to be very stable, as confirmed by the binding energy and their differentials. Doye and Wales[19] also reported that Ni_{13} and Ni_{55} nanoclusters have icosahedral structures. In their study, Singh and Kroll[26] performed ab initio geometry optimization of clusters for 13, 55, and 147 atoms of Fe, Co, and Ni using the spin-polarized density functional theory (DFT) and generalized gradient approximation (GGA) implemented in the Vienna Ab-initio Simulation Package (VASP). It was also reported that icosahedral structures had lower energies than other structures at all total magnetic moments. It was implied that the cohesive energy of a cluster increased with the increasing size of cluster. Onal et al.[27] investigated Ni_2 dimers and Ni_{13} nanoclusters quantum mechanically in terms of their structures, binding energies, and bond lengths by use of the DFT/B3LYP method with 3 different basis sets.

Carbon monoxide and oxygen adsorption on nanosized gold particles such as Au_{10} nanoclusters and on Au(111) and Au(210) single-crystal surfaces were studied quantum mechanically by Lopez et al.[28] Their DFT calculations indicated that CO and O_2 adsorption energies increased proportionately with decreasing coordination numbers (CNs) of surface gold atoms. As a result, they concluded that the chemical activity of gold was strongly dependent on the CN of the gold atoms. Meanwhile, van Santen and Neurock[29] emphasized that metal atoms in clusters with very low CNs formed very strong bonds with the adsorbate to compensate for the smaller number of metal-metal bonds. This increased the binding energy between the metal and the adsorbate. Yilmazer et al.[30] theoretically investigated the ethylene adsorption on a Ni_{13} nanocluster and different nickel surfaces with different CNs by use of DFT with B3LYP formalism. It was reported that ethylene adsorption energy increased with decreasing Ni CNs.

The primary aim of this study was to perform equilibrium geometry calculations for a Ni_{55} nanocluster by using the DFT/B3LYP method. The results were compared with other theoretical and experimental data in terms of geometric structure and binding energy/atom values. In addition, for 2 CNs, a comparison of ethylene adsorption energies on a Ni_{55} nanocluster with π-adsorption mode was made as a function of the CN of the Ni atom of the active site.

Nanocluster model and theoretical approach

All calculations in this study were based on DFT[31] implemented in the Gaussian 03 suite of programs.[32] To take into account the exchange and correlation term, B3LYP[33–35] formalism was used in this study. The 6-31G(d,p) basis set was used for C and H atoms and the 86-411(41d)G basis set was utilized for Ni atoms. The 86-411(41d)G basis set was chosen for Ni atoms since it was reported by Towler et al. that the structural, elastic, and vibrational properties were in reasonable agreement with the related experimental data.[36] Extended Gaussian basis sets were generated for 27 atomic orbitals for Ni, where each orbital is a linear combination

(contraction) of Gaussian-type functions. It was demonstrated[37] that the hybrid B3LYP method is a high-quality density functional method for use in organic chemistry, and also that the application of the hybrid basis sets predicted correct geometries for large cluster systems.[38,39] Moreover, for structures containing transition metal atoms, the B3LYP functional gives precise binding energies, whereas it yields somewhat short bond lengths.[40–42]

Related to the construction of the Ni_{55} nanoclusters, it is known that the first magic-number cluster following the nickel dimer is Ni_{13}. Magic-number clusters are generally obtained by surrounding 1 single metal atom with metal atom layers by obeying the formula $y = 10n^2 + 2$ suggested by Schmid[43] where y is the total number of atoms at the nth layer. Ni_{13} clusters are known to be developed by surrounding 1 single nickel atom with 12 nickel atoms conforming with the Mackay icosahedral structure as suggested theoretically[5,13,14,44,45] and experimentally.[46] Similarly, for the construction of our Ni_{55} nanocluster, input geometry was set up from a Ni_{13} nanocluster by adding a second layer according to the formula $y = 10n^2 + 2$. It was mentioned by Lathiotakis et al.[13] and Luo[23] that Jahn-Teller distortions of electronically degenerate configurations play an important role in the full optimization of nickel clusters. It was explicitly noted that a wrong structure for nickel clusters could be found by ignoring directional bonding in the d manifold in equilibrium geometry calculations.[23] Hence, the quantum mechanical calculations included JahnTeller distortions without using any symmetry constraint.

Quantum mechanical investigations consist of structural information and the total system energy for the optimum geometry of the considered cluster. In order to convert the calculated total energy of the cluster to the atomic binding energy, the following formula was used

$$\text{Binding energy } \left({}^{eV}/_{\text{atom}}\right) = \frac{[\text{Total energy of } Ni_n \text{ cluster}] - n * [\text{Single } Ni \text{ atom energy}]}{n}$$

Table 1. Values of binding energy and bond length of Ni_{55} nanocluster.

References	Method	(eV/atom) Binding energy	Mean distance (Å)
Lathiotakis et al.[13]	TBMD	4.27	2.59
Luo[23]	TBMD	3.55	2.45
Grigoryan and Springborg[16]	EAM	3.83	2.59
Montejano-Carrizales et al.[18]	EAM	3.87	-
Wang et al.[22]	DFT	3.92	2.45 2.52
Kar'kin et al.[24]	MD	3.69[a]	-
Xiang et al.[25]	GSA	3.77	2.36
Singh and Kroll[26]	DFT	4.54	2.35 (interatomic) 2.47 (1st shell) 2.41 (2nd shell)
This study	DFT	3.51	2.49

[a]From graph in related reference.

Here, n is the number of atoms in the cluster. It should be noted that the quantum mechanical calculation method was kept the same for both the single atom and the cluster.

The parameter of $n^{-1/3}$, where n is the number of atoms in the cluster, generally provides a linear relationship with the binding energy of clusters. The intercept of the resulting line with the binding energy axis provides a theoretical estimate for the probable binding energy of bulk nickel with an infinite number of atoms. In this study, the computed binding energy of the Ni_{55} nanocluster was used together with previous data from the literature[27] including the binding energies of Ni_2 (dimer) and Ni_{13} nanoclusters, to investigate the above correlation. These findings were also compared with previous experimental and theoretical data from the literature.

All atoms were kept relaxed in all directions and their electrons were not kept frozen in this study. Equilibrium geometry (EG) calculations were performed for the determination of the binding energy of nickel and the adsorption energy of ethylene. Computed <S2> values confirmed that the spin contamination was very small (maximum: 0.9% after annihilation). Convergence criteria were the gradients of maximum force, root-mean-square (rms) force, maximum displacement, and rms displacement, and these were found in Gaussian 03 to be 0.000450, 0.000300, 0.001800, and 0.001200, respectively.

The computational strategy employed in this study was as follows Initially, the correct spin multiplicity (SM) of the nanocluster and adsorbing molecule was determined by single point energy (SPE) calculations. SPE values were also calculated with different SM numbers for the nanocluster system which included the adsorbing molecule. The SM number that corresponded to the lowest SPE was accepted as the correct SM. The cluster and the adsorbing molecule, ethylene, were then fully optimized geometrically by means of EG calculations. The relative adsorption energy was defined by the following formula:

$$\Delta E = E_{\text{system}} - (E_{\text{cluster}} + E_{\text{adsorbate}})$$

where E_{system} is the calculated equilibrium energy of the given geometry containing the cluster and the adsorbing molecule; $E_{cluster}$ is the energy of the cluster; and $E_{adsorbate}$ is the energy of the adsorbing molecule, which was ethylene in this case.

Results and discussion

Optimization and binding energy of Ni_{55} nanocluster

Geometry optimization calculations for the magic-number cluster of Ni_{55} were carried out using the DFT method in Gaussian 03. The SM number of the nanocluster was 11, corresponding to the lowest energy. The EG calculation for the Ni_{55} nanocluster, which was carried out without using any symmetry constraints and by allowing for Jahn-Teller deformations, resulted in a distorted icosahedral geometry structure using the DFT method. The optimized geometry of the Ni_{55} nanocluster is shown in Figure 1. Figure 2 represents the EG of the nanocluster with the details of the cluster geometry. The resultant geometry was found with the Jahn-Teller distortions as also suggested experimentally[5,6] and theoretically.[13,23]

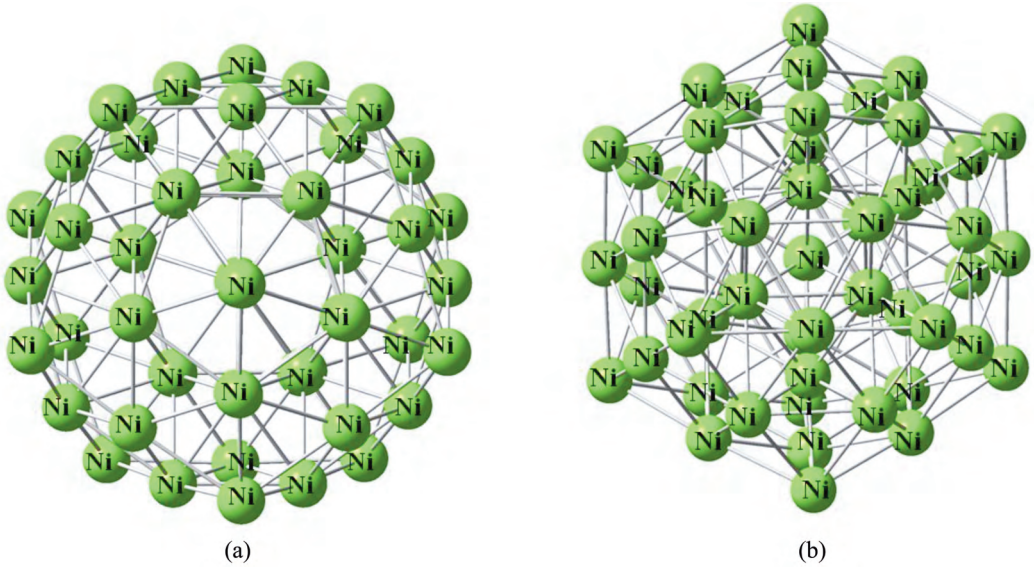

Figure 1. Optimized Ni_{55} nanocluster with ball and bond representation: a) top view, b) side view.

As indicated in Figure 2, for the Ni_{55} nanocluster, the average bond distance between the first shell and the center atom was computed as 2.43 ± 0.02 Å. The average bond distance between the atoms in the first shell and the other atoms neighboring them, including the center atom and the second-shell atoms, was 2.49 ± 0.01 Å. Finally, the average bond distance considering only vertex atoms in the outer (second) shell and the atoms neighboring those was 2.56 ± 0.03 Å.

The mean cluster bond length was calculated to be 2.49 Å for the Ni_{55} nanocluster. Corresponding theoretical mean cluster bond length values were reported as 2.59,[13] 2.45, [23] 2.59,[16] 2.45 and 2.52[22] 2.36[25] and 2.35, 2.47 and 2.41 Å.[26] Although there are some differences among the bond length values, these values are in reasonable agreement with each other as different theoretical methods were used. All bond length values are shown in Table 1.

In addition, the binding energy of the Ni_{55} nanocluster was computed as 3.51 eV/atom which is in reasonable agreement with other theoretical binding energy values for Ni_{55} nanoclusters. Values of 3.55[23] and 4.27[13] eV/atom were obtained by the TBMD method, 3.83[16] and 3.87[18] eV/atom by the EAM method, 3.92[22] eV/atom by the VASP/Perdew-Burke-Ernzerhof (PBE) method, 3.69[24] eV/atom by the MD method, 3.77[25] eV/atom by the GSA method and 4.54 [26] eV/atom by the DFT method.

Binding energy relation among icosahedral nanoclusters: Ni_2 dimer and Ni_{13} and Ni_{55} nanoclusters

For binding energy considerations, a correlation line was drawn and the intercept of the binding energies was obtained against the value of $n^{-1/3}$ for the cluster. The parameter of $n^{-1/3}$, where n is the number of atoms in the cluster, generally provided a linear relationship with the binding energy of the clusters. The intercept of the resulting line with the binding energy axis provides a theoretical estimate for the probable binding energy of bulk nickel with an infinite number of atoms as stated previously.

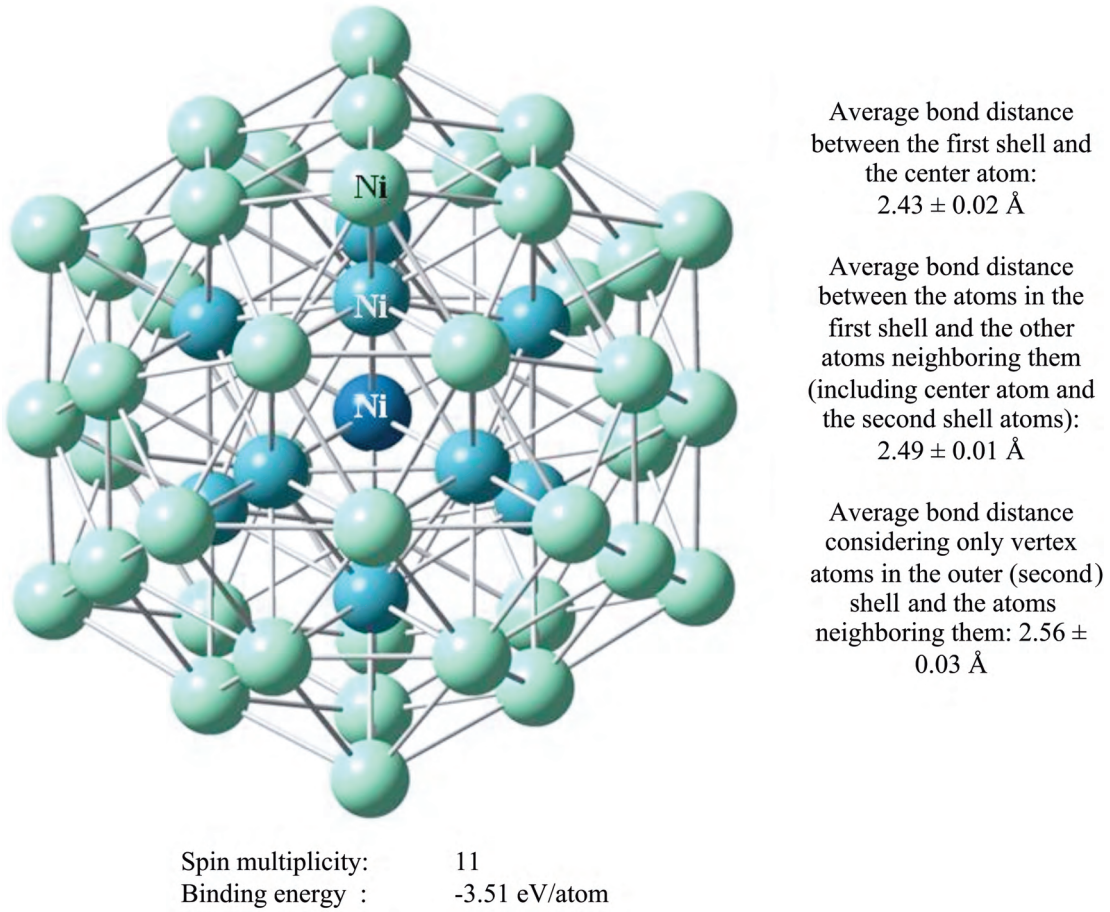

Figure 2. Optimized Ni_{55} nanocluster with the distance of nickel atoms of the shells and binding energy (darkest atom is the core/center Ni atom, medium-dark Ni atoms are the first layer of the cluster, and the lightest surrounding Ni atoms are the second-layer atoms).

In this work, the computed binding energy data of the Ni_2 dimer and Ni_{13} nanocluster from our previous study[27] were considered together with the binding energy of the Ni_{55} nanocluster obtained in this study for the investigation of the above correlation. Theoretical binding energies for the Ni_2 dimer and Ni_{13} and Ni_{55} nanoclusters and their intercepts including the results obtained in this study and other theoretical values reported in the literature[13,16,22,23,25–27,47–49] are given in Table 2.

Figure 3 was plotted by taking the theoretical binding energies for the Ni_2 dimer, Ni_{13} and Ni_{55} according to the available data reported in Table 2, where the trend line for our data is shown with a bold black line. This study's corresponding extrapolation for the bulk value was 4.85 eV/atom, a good estimation for the bulk nickel binding energy at an infinite value of N; this experimental value was reported as 4.45 eV/atom by Voter and Chen.[50]

It can be seen in the literature that techniques affecting the accuracy of the results have been used to obtain the binding energy of bulk nickel. For instance, Lathiotakis et al.[13] obtained an overestimated bulk value of 5.69 eV/atom by using the minimal parameter TBMD method. On the contrary, Luo[23] preferred TBMD

Table 2. Binding energy values for Ni_2 dimer and Ni_{13} and Ni_{55} nanoclusters.

References	Method	Binding energy (eV/atom)			
		Ni_2	Ni_{13}	Ni_{55}	Intercept
Calleja et al.[47]	DFT/double-ζ bases	1.20	2.76		4.56
Lathiotakis et al.[13]	TBMD (minimal parameter)	0.93	3.16	4.10	5.69
Luo[23]	TBMD (simulated annealing)	-	2.99	3.55	4.45
Grigoryan and Springborg[16]	EAM	1.81	3.38	3.83	4.93
Reuse and Khanna[48]	DFT/LSD[b]	1.61	4.26		7.32
Wang et al.[22]	DFT/PBE	2.23	3.33	3.92	4.08
Xiang et al.[25]	GSA	2.11[a]	3.38[a]	3.77	
Singh and Kroll[26]	DFT/FS potential	-	3.84	4.51	
Yao et al.[49]	DFT/GGA	-	3.87[a]	4.57[a]	
Onal et al.[27]	DFT/B3LYP/ m6-31 G*	1.08	2.70	-	4.57
	DFT/B3LYP/ 6-31 G**	0.66	2.86	-	5.39
	DFT/B3LYP/ 86-411(41d)G	1.16	3.11		
This study	DFT/B3LYP/ 86-411(41d)G			3.51	4.85
Voter and Chen[50]	Experimental (bulk)		4.45		

[a]From graph in related references.

[b]Local spin density.

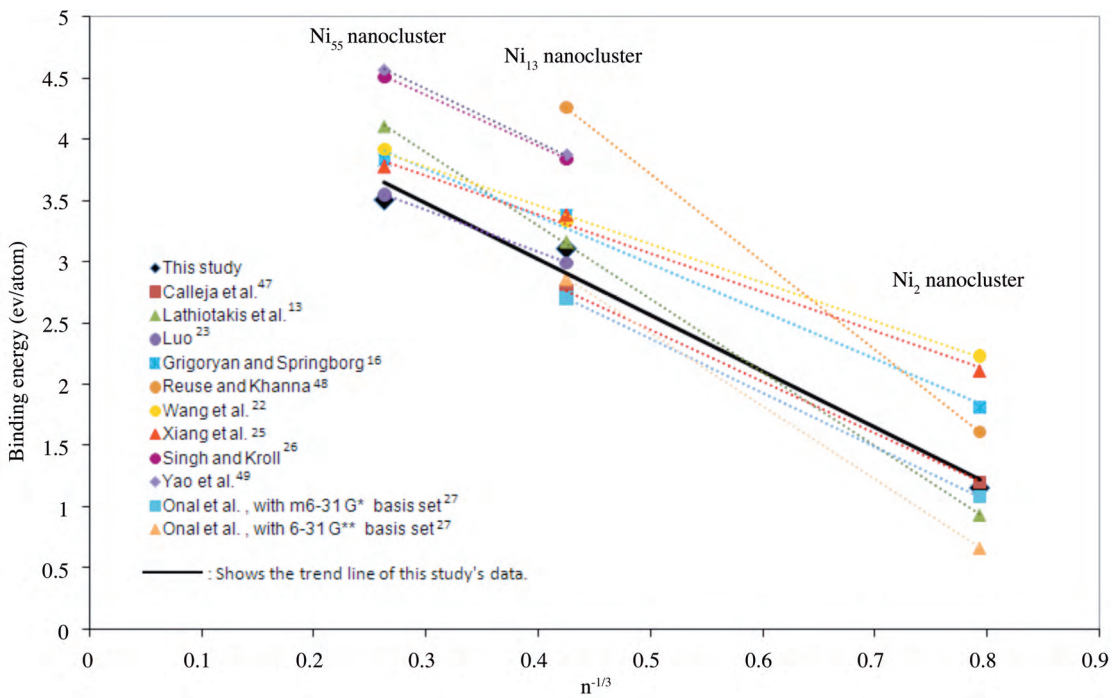

Figure 3. Binding energy relation as a function of $n^{-1/3}$ for magic-number clusters Ni_2 dimer, Ni_{13} nanocluster, and Ni_{55} nanocluster, where n is the number of atoms in the cluster, as obtained in this study and in reported literature.

with the simulated annealing technique achieving a value of 4.45 eV/atom. It is also possible that the inclusion of Ni_{55} results may have improved the correlation compared to results based only on the Ni_2 dimer and Ni_{13} nanocluster.

Ethylene adsorption on Ni_{55} nanocluster

The EG for C_2H_4 as an adsorbing molecule was obtained by assuming the total charge to be neutral with a singlet spin multiplicity. The C–C and C–H distances were computed as 1.330 Å and 1.087 Å, respectively. The corresponding experimental values were reported as 1.337 Å[51] and 1.34 Å[52] for the C–C distance and 1.103 Å[50] and 1.10 Å[52] for the C–H distance.

The Ni_{55} nanocluster has 2 alternative adsorption sites with CNs of 6 and 8 that can be considered for the cluster surface geometry. Ethylene adsorption was studied with the π-adsorption mode for both CNs on the Ni_{55} nanocluster in this study. The adsorption energy was computed as –0.87 eV for CN 6. The optimized geometry of this type of adsorption is shown in Figure 4. The adsorption energy for CN 8 was calculated to

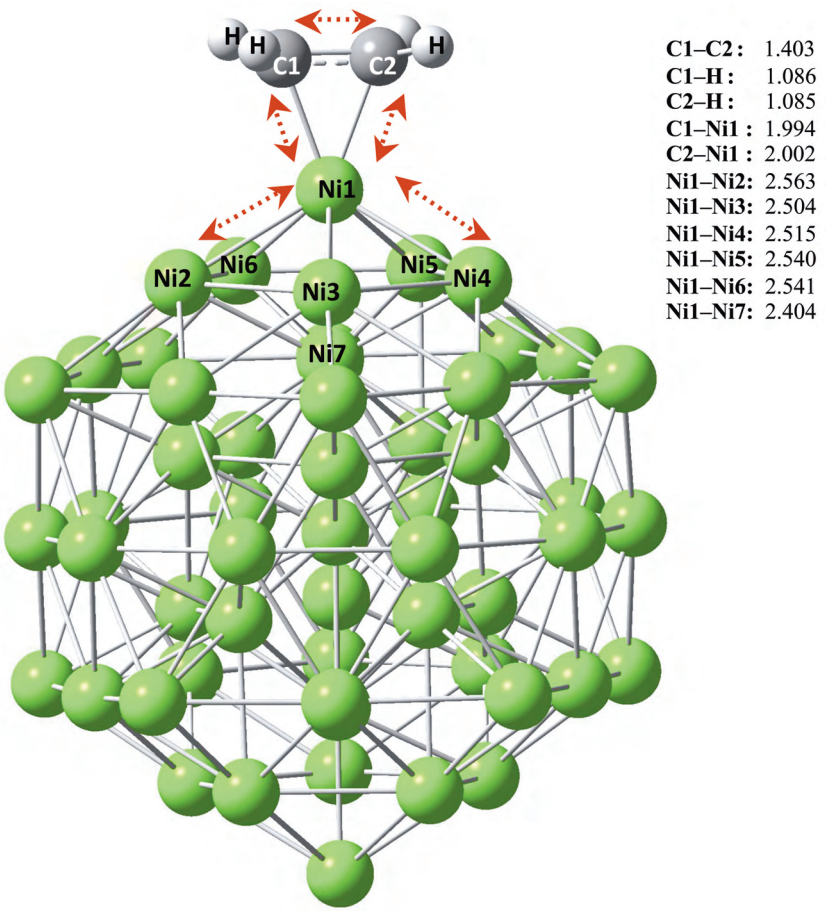

Figure 4. Equilibrium geometry of adsorbed ethylene on Ni_{55} nanocluster with CN 6 by π-adsorption mode (values are in units of Å).

be –0.68 eV, and the optimized adsorption geometry is shown in Figure 5. Presently, there is no theoretical or experimental study concerning ethylene adsorption on Ni_{55} nanoclusters in the literature.

It was reported[53] that for most metals, 2 general types of low-temperature spectra have been reliably identified and assigned to 2 distinct nondissociative adsorption modes of ethylene. These are the di-σ adsorption and π-adsorption modes. In the di-σ adsorption mode, the ethylene molecule interacts directly with 2 metal atoms, while it interacts with a single metal atom in the π-adsorption mode. It was claimed that, in some cases, both types of species coexist; in other cases, one type occurs on one crystal surface of a given metal and the other occurs on a different one. In our study, only the π-adsorption mode of ethylene was observed on the Ni_{55} nanocluster for both coordination numbers. Even though a slight tendency for a hybrid adsorption mode was noticed on the nanocluster, the di-σ adsorption mode was not examined in a complete manner on the Ni_{55} nanocluster.

It can be stated that ethylene adsorption energy increases from 0.68 to 0.87 eV with Ni CNs decreasing from 8 to 6 for the Ni_{55} nanocluster. It was already mentioned[29] that the adsorbate bond energy increases with an increase in the degree of coordinatively unsaturated metal atoms. This is also due to the decrease in the localization energy of electrons on the surface metal atoms for structures with fewer neighboring atoms. It was further observed that the atomic charge (+0.106) of Ni atoms with CN = 6 is relatively higher than the charge value of +0.006 for Ni atoms with CN = 8. In our previous study,[30] a similar trend was observed for ethylene

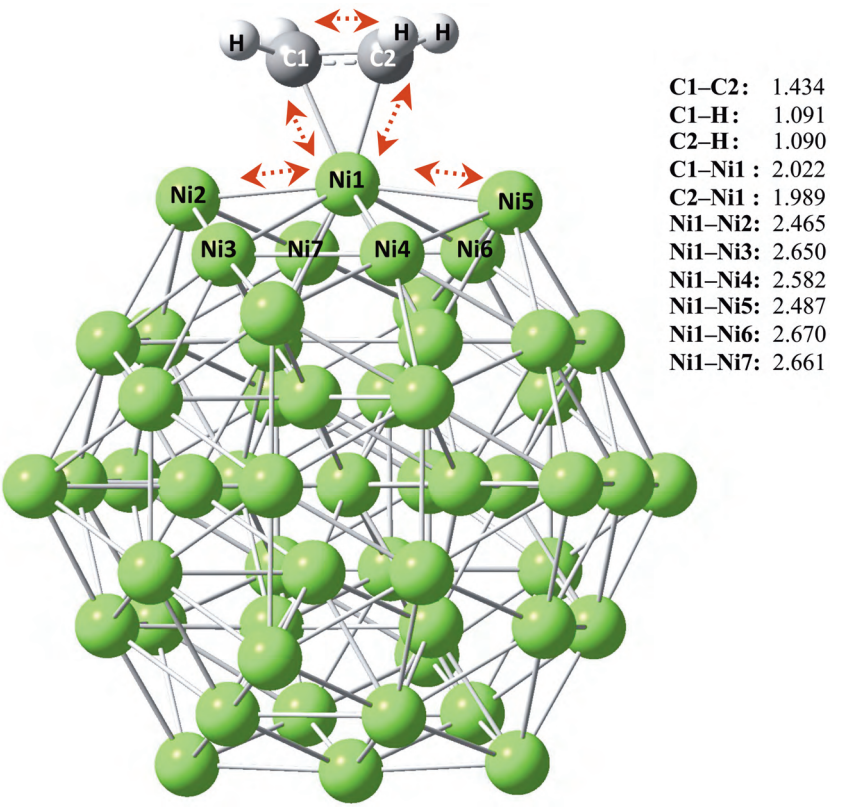

Figure 5. Equilibrium geometry of adsorbed ethylene on Ni_{55} nanocluster with CN 8 by π-adsorption mode (values are in units of Å).

adsorption with different CNs for different nickel surface clusters and for Ni_{13} nanoclusters in another basis set, 6-31G(d,p), in Gaussian 03 by use of DFT with B3LYP formalism. This type of correlation was also mentioned between the metal atoms and an adsorbate in studies by Lopez et al.[28] and van Santen and Neurock.[29]

Conclusions

Optimizations of a Ni_{55} nanocluster and ethylene adsorption were studied by means of the DFT/B3LYP method. Equilibrium geometry calculations for the Ni_{55} cluster resulted in the lowest binding energy of 3.51 eV/atom, which led to an intercept value of 4.85 eV/atom together with correlations considering the Ni_2 dimer and Ni_{13} nanoclusters from our previous study. The calculated intercept value which actually refers to the theoretical bulk value of the binding energy of nickel was in reasonable agreement with the experimental bulk value of 4.45 eV/atom.

In addition, ethylene adsorption energies were obtained for the Ni_{55} nanocluster as approximately –0.87 eV and –0.68 eV for CNs 6 and 8, respectively. It can be stated that ethylene adsorption energy increases with as the CN of Ni decreases from 8 to 6.

Acknowledgments

The numerical calculations reported in this paper were performed at the TÜBİTAK ULAKBİM High Performance and Grid Computing Center (TR-Grid e-Infrastructure).

References

1. Grigoryan, V. G.; Springborg, M. *Phys. Chem. Chem. Phys.* **2001**, *3*, 5135-5139.
2. Schmid, G.; Maihack, V.; Lantermann, F.; Peschel, S. *J. Chem. Soc. Dalton Trans.* **1996**, *5*, 589-595.
3. Winter, B. J.; Klots, T. D.; Parks, E. K.; Riley, S. J. *Z. Phys. D Atom. Mol. Cl.* **1991**, *19*, 375-380.
4. Klots, T. D.; Winter, B. J.; Parks, E. K.; Riley, S. J. *J. Chem. Phys.* **1991**, *95*, 8919-8930.
5. Pellarin, M.; Baguenard, B.; Vialle, J. L.; Lerme, J.; Broyer, M.; Miller, J.; Perez, A. *Chem. Phys. Lett.* **1994**, *217*, 349-356.
6. Parks, E. K.; Winter, B. J.; Klots, T. D.; Riley, S. J. *J. Chem. Phys.* **1991**, *94*, 1882-1902.
7. Parks, E. K.; Zhu, L.; Ho, J.; Riley, S. J. *J. Chem. Phys.* **1994**, *100*, 7206-7222.
8. Parks, E. K.; Zhu, L.; Ho, J.; Riley, S. J. *J. Chem. Phys.* **1995**, *102*, 7377-7389.
9. Parks, E. K.; Riley, S. J. *Z. Phys. D* **1995**, *33*, 59-70.
10. Daw, M. S.; Foiles, S. M.; Baskes, M. I. *Mater. Sci. Rep.* **1993**, *9*, 251-310.
11. Norskov, J. K. *Prog. Surf. Sci.* **1991**, *38*, 103-144.
12. Christensen, A.; Stoltze, P.; Norskov, J. K. *J. Phys. Condens. Matter* **1995**, *7*, 1047-1057.
13. Lathiotakis, N. N.; Andriotis, A. N.; Menon, M.; Connolly, J. *J. Chem. Phys.* **1996**, *104*, 992-1003.

14. Stave, M. S.; DePristo, A. E. *J. Chem. Phys.* **1992**, *97*, 3386-3389.
15. Wetzel, T. L.; DePristo, A. E. *J. Chem. Phys.* **1996**, *105*, 572-580.
16. Grigoryan, V. G.; Springborg, M. *Chem. Phys. Lett.* **2003**, *375*, 219-226.
17. Montejano-Carrizales, J. M.; Iñiguez, M. P.; Alonso, J. A. *J. Cluster Sci.* **1994**, *5*, 287-302.
18. Montejano-Carrizales, J. M.; Iñiguez, M. P.; Alonso, J. A.; Lopez, M. J. *Phys. Rev. B* **1996**, *54*, 5961-5969.
19. Doye, J. P. K.; Wales, D. J. *New J. Chem.* **1998**, *22*, 733-744.
20. Cleveland, C. L.; Landman, U. *J. Chem. Phys.* **1991**, *94*, 7376-7396.
21. Qi, Y.; Çağin, T.; Johnson, W. L.; Goddard, W. A. *J. Chem. Phys.* **2001**, *115*, 385-394.
22. Wang, Q.; Lim, K. H.; Yang, S. W.; Yang, Y.; Chen, Y. *Theor. Chem. Acc.* **2011**, *128*, 17-24.
23. Luo, C. *Model. Simul. Mater. Sci.* **2002**, *10*, 13-20.
24. Kar'kin, I. N.; Kar'kina, L. E.; Gornostyrev, Yu. N. *Phys. Metals Metallogr.* **2008**, *106*, 260-265.
25. Xiang, Y.; Sun, D. Y.; Gong, X. G. *J. Phys. Chem. A* **2000**, *104*, 2746-2751.
26. Singh, R.; Kroll, P. *Phys. Rev. B* **2008**, *78*, 245404.
27. Onal, I.; Sayar, A.; Uzun, A.; Ozkar, S. *J. Comput. Theor. Nanosci* **2009** *6* 867872.
28. Lopez, N.; Janssens, T. V. W.; Clausen, B. S.; Xu, Y.; Mavrikakis, M.; Bligaard, T.; Norskov, J. K. *J. Catal.* **2004** *223*, 232235.
29. van Santen, R. A.; Neurock, M. *Molecular Heterogeneous Catalysis*, Wiley-VCH, Weinheim, 2006.
30. Yilmazer, N. D.; Fellah, M. F.; Onal, I. *Appl. Surf. Sci.* **2010**, *256*, 5088-5093.
31. Kohn, W.; Sham, L. J. *Phys. Rev.* **1965** *140*, A1133A1138.
32. Frisch, M. J.; Trucks, G. W.; Schlegel, H. B.; Scuseria, G. E.; Robb, M. A.; Cheeseman, J. R.; Montgomery, J. A. Jr.; Vreven, T.; Kudin, K. N.; Burant, J. C.; Millam, J. M.; Iyengar, S. S.; Tomasi, J.; Barone, V.; Mennucci, B.; Cossi, M.; Scalmani, G.; Rega, N.; Petersson, G. A.; Nakatsuji, H.; Hada, M.; Ehara, M.; Toyota, K.; Fukuda, R.; Hasegawa, J.; Ishida, M.; Nakajima, T.; Honda, Y.; Kitao, O.; Nakai, H.; Klene, M.; Li, X.; Knox, J. E.; Hratchian, H. P.; Cross, J. B.; Bakken, V.; Adamo, C.; Jaramillo, J.; Gomperts, R.; Stratmann, R. E.; Yazyev, O.; Austin, A. J.; Cammi, R.; Pomelli, C.; Ochterski, J. W.; Ayala, P. Y.; Morokuma, K.; Voth, G. A.; Salvador, P.; Dannenberg, J. J.; Zakrzewski, V. G.; Dapprich, S.; Daniels, A. D.; Strain, M. C.; Farkas, O.; Malick, D. K.; Rabuck, A. D.; Raghavachari, K.; Foresman, J. B.; Ortiz, J. V.; Cui, Q.; Baboul, A. G.; Clifford, S.; Cioslowski, J.; Stefanov, B. B.; Liu, G.; Liashenko, A.; Piskorz, P.; Komaromi, I.; Martin, R. L.; Fox, D. J.; Keith, T.; Al-Laham, M. A.; Peng, C. Y.; Nanayakkara, A.; Challacombe, M.; Gill, P. M. W.; Johnson, B.; Chen, W.; Wong, M. W.; Gonzalez, C.; Pople, J. A. Gaussian 03 Gaussian, Inc. Wallingford, CT, 2003.
33. Becke, A. D. *Phys. Rev. B* **1988**, *38*, 30983100.
34. Becke, A. D.; Roussel, M. R. *Phys. Rev. A* **1989**, *39*, 37613767.
35. Lee, C.; Yang, W.; Parr, R. G. *Phys. Rev. B* **1988**, *37*, 785789.
36. Towler, M. D.; Allan, N. L.; Harrison, N. M.; Saunders, V. R.; Mackrodt, W. C.; Apra, E. *Phys. Rev. B* **1994**, *50*, 5041-5054.
37. Baker, J.; Muir, M.; Andzelm, J.; Scheiner, A. *ACS Symposium Series* **1996**, *629*, 342-367.
38. Zhang, R. Q.; Wong, N. B.; Lee, S. T.; Zhu R. S.; Han, K. L. *Chem. Phys. Lett.* **2000** *319*, 213-219.
39. Zhang, R. Q.; Xie, X. G.; Liu, S. X.; Lee C. S.; Lee, S. T. *Chem. Phys. Lett.* **2000** *330*, 484-490.

40. Zdetsis, A. D.; Koukaras, E. N.; Garoufalis, C. S. *J. Math. Chem.* **2009**, *46*, 971-980.
41. Stephens, P. J.; Devlin, F. J.; Chabalowski, C. F.; Frisch, M. J. *J. Phys. Chem.* **1994**, *98*, 11623-11627.
42. Yanagisawa, K.; Tsuneda, T.; Hirao, K. *J. Chem. Phys.* **2000**, *112*, 545-553.
43. Schmid, G. *Chem. Rev.* **1991**, *92*, 1709-1727.
44. Raghavan, K.; Stave, M. S.; DePristo, A. E. *J. Chem. Phys.* **1989**, *91*, 1904-1917.
45. Northby, J. A. *J. Chem. Phys.* **1987**, *87*, 6166-6177.
46. Nayak, S. J.; Khanna, S. N.; Rao, B. K.; Jena, P. *J. Phys. Chem.* **1997**, *101*, 1072-1080.
47. Calleja, M.; Rey, C.; Alemany, M. M. G.; Gallego, L. J.; Ordejon, P.; Sanchez-Portal, D.; Artacho, E.; Soler, J. M. *Phys. Rev. B* **1999**, *60*, 2020-2024.
48. Reuse, F. A.; Khanna, S. N. *Chem. Phys. Lett.* **1995**, *234*, 77-81.
49. Yao, Y. H.; Gu, X.; Ji, M.; Gong, X. G.; Wang, D. *Phys. Lett. A* **2007**, *360*, 629-631.
50. Voter, A. F.; Chen, S. P. *Mater. Res. Soc. Symp. Proc.* **1987**, *82*, 175-180.
51. Kuchitsu, K. In *Structure Data of Polyatomic Molecules*; Kuchitsu, K., Ed.; Springer-Verlag, Berlin, 1992
52. Sundaram, K. M.; Shreehan, M. M.; Olszewski, E. F. *Kirk-Othmer Encyclopedia of Chemical Technology*, Vol. 10, Wiley, Hoboken, NJ, 2001.
53. Bernardo, G. P. M.; Gomes, J. A. N. F. *Theoretical Aspects of Heterogeneous Catalysis*, Kluwer Academic Publishers, Netherlands, 2001.